

The Berezinskii-Kosterlitz-Thouless Transition and Anomalous Metallic Phase in a Hybrid Josephson Junction Array

C. G. L. Bøttcher,^{1,*} F. Nichele,^{1,†} J. Shabani,^{2,‡} C. J. Palmstrøm,^{2,3,4} and C. M. Marcus¹

¹*Center for Quantum Devices, Niels Bohr Institute,
University of Copenhagen, 2100 Copenhagen, Denmark*

²*California NanoSystems Institute, University of California, Santa Barbara, CA 93106, USA*

³*Department of Electrical Engineering, University of California, Santa Barbara, CA 93106, USA*

⁴*Materials Department, University of California, Santa Barbara, CA 93106, USA*

(Dated: October 4, 2022)

We investigate the Berezinskii-Kosterlitz-Thouless (BKT) transition in a semiconductor-superconductor two-dimensional Josephson junction array. Tuned by an electrostatic top gate, the system exhibits separate superconducting (S), anomalous metal (M*), and insulating (I) phases, bordered by separatrices of the temperature-dependent of sheet resistance, R_s . We find that the gate-dependent BKT transition temperature falls to zero at the S-M* boundary, suggesting incomplete vortex-antivortex pairing in the M* phase. In the S phase, R_s is roughly proportional to perpendicular magnetic field at the BKT transition, as expected, while in the M* phase R_s deviates from its zero-field value as a power-law in field with exponent close to 1/2 at low temperature. An in-plane magnetic field eliminates the M* phase, leaving a small scaling exponent at the S-I boundary, which we interpret as a remnant of the incipient M* phase.

Josephson junction arrays (JJAs) have for decades provided model systems for investigating classical and quantum phase transitions with competing ground states, frustration, and complex dynamics [1, 2], 2D superconductivity [3, 4], and more recently as a basis for quantum simulation [5], quantum matter [6], and protected quantum information [7, 8]. It is generally accepted that JJAs exhibit a quantum phase transition between superconducting and insulating phases controlled by the ratio E_C/E_J of charging energy, E_C , of a single island to the Josephson energy, E_J , between neighboring islands. At the superconductor-insulator transition (SIT), the 2D sheet resistance R_s of the JJA is roughly the resistance quantum, $R_s \sim R_Q \equiv h/4e^2$ [9, 10], or equivalently, $E_C/E_J \sim 1$, with a temperature-independent separatrix at $R_s \sim R_Q$ [1, 2].

However, this conventional SIT picture misses a commonly observed regime seen in a variety of materials—the anomalous metal—where R_s saturates at low temperature at a tunable value $R_s < R_Q$ [11]. The origin and requirements for the anomalous metal are not known, despite years of investigation and speculation [11–15].

At zero magnetic field, temperature destroys 2D superconductivity through a Berezinskii-Kosterlitz-Thouless (BKT) transition, characterized by the unbinding of vortex-antivortex pairs when the temperature, T , exceeds a critical value, T_{BKT} [17–19]. Dissipation by the motion of unbound vortices above T_{BKT} results in nonzero resistivity [20, 21].

In this Letter, we experimentally investigate the interaction of the BKT transition with the anomalous metal in an InAs/Al heterostructure patterned into a regular array of micron-size Al islands separated by narrow stripes where the Al has been removed, which can be depleted by a global gate. We identify two distinct boundaries

where $R_s(T)$ curves separate, controlled by gate voltage, defining three regions of superconducting (S), anomalous metal (M*) and insulating (I) phases. A similar conclusion was recently proposed for a field-driven SIT [22, 23], and contrasts interpretations where BKT crosses to a quantum-dominated regime throughout the superconducting phase [24], or where inadequate cooling is responsible for anomalous metal behavior [25, 26].

We find that in S phase, that is, the low-resistance side of the S-M* separatrix, the temperature dependent sheet resistance, $R_s(T)$, is well described by the BKT form [20] over three orders of magnitude of R_s , yielding a gate-voltage-dependent T_{BKT} as a fit parameter. Importantly, we find T_{BKT} goes to zero at the S-M* boundary, *not* at the T -independent separatrix (our M*-I boundary) where $R_s \sim R_Q$, as one would expect for a conventional SIT [2, 27]. The observation of a vanishing T_{BKT} at the S-M* boundary suggests that the transition from M* to the normal metal (M) with increasing temperature is not BKT-like. We interpret the result as incomplete vortex-antivortex pairing that persists to zero temperature in the M* phase.

We next demonstrate power-law dependences of R_s on small perpendicular field, B_\perp , in both the S and M* phases. Linear magnetoresistance, $R_s(B_\perp, T_{\text{BKT}}) \propto B_\perp^\beta$, with $\beta = 1$, is expected around the BKT transition [28–32]. We find that in the S phase, $\beta(T) \sim 1$ near T_{BKT} , though we find $\beta(T)$ increasing with T , contrary to [28, 29]. In the M* phase, beyond where $T_{\text{BKT}} \rightarrow 0$, we again find a power law after subtracting the saturation value, $[R_s(B_\perp, T) - R_s(0, T)] \propto B_\perp^\beta$, though with $\beta < 1$, approaching $\beta = 1/2$ well into M* [see Figs. 3(b,c)].

Finally, we find that a moderate in-plane magnetic field, $B_\parallel \sim 0.5$ T, known to eliminate M* [16], causes the S-M* and M*-I phase boundaries to coalesce into to a single broad S-I boundary (Fig. 4). The broad S-I transition

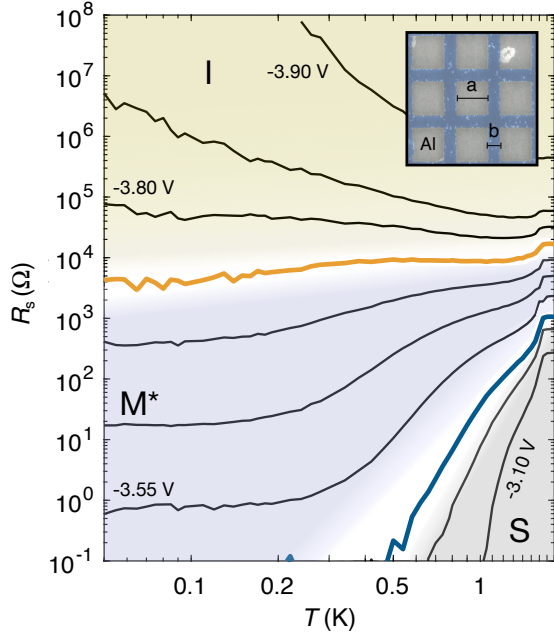


FIG. 1. Sheet resistance, $R_s(T)$, of the InAs/Al Josephson junction array (inset) as a function of temperature, T , at several gate voltages, V_G , ranging from -3.1 V to -3.9 V, from Ref. [16]. Two separatrixes (blue and orange curves) mark the boundaries between superconducting (S) phase, where $R_s(T)$ is concave down, becoming unmeasurably small at low T , the anomalous metal (M^*), where $R_s(T)$ is concave up and saturating at low T , and the insulating phase, where $R_s(T)$ increases with falling T . The S- M^* boundary (blue) starts at normal-state sheet resistance, $R_N \sim 1$ k Ω . The M^* -I (orange) is roughly temperature independent, with $R_s \sim 6$ k Ω , similar to with a conventional S-I boundary. Inset: false-color electron micrograph with scale bar showing the array before the deposition of the top insulator and metallic gate, with $1 \mu\text{m}$ Al squares patterned onto an InAs substrate, as described in Ref. [16].

at $B_{\parallel} = 0.5$ T shows a small scaling exponent at low- T , a possible remnant of the M^* phase. A transition from slow and fast temperature dependence is seen toward the S side of the broad S-I transition, separated from the S-I crossing point at $R_s \sim R_Q$, presumably another vestige of the M^* phase. The JJA was fabricated using a hybrid InAs/Al heterostructure, with a 7 nm InAs quantum well separated from a 7 nm epitaxial Al surface layer by 10 nm InGaAs barrier [16]. A Hall bar was patterned by wet etching through the quantum well. A subsequent patterning of 40×100 array of $1 \mu\text{m}$ Al squares separated by 150 nm (Device A) or 350 nm (Device B) spacing was patterned by removing the Al between squares using Transene D aluminum etchant (see Fig. 1, inset). The array was then covered by a 40 nm Al_2O_3 insulating layer followed by a Ti/Au top gate. The two measured devices behaved similarly. Except where noted data are from Device A.

Devices were measured in a dilution refrigerator with

a base mixing chamber temperature of 20 mK. A vector magnet was used to independently apply perpendicular and in-plane magnetic fields applied along the current direction, after calibrating the magnet axes to compensate for small sample tilt. A four-wire measurement of longitudinal resistance with both current and voltage measured was carried out using standard AC lock-in techniques, keeping the voltage across the array below $5 \mu\text{V}$. 2D sheet resistance $R_s(T)$, spanning 0.1Ω to $100 \text{ M}\Omega$, were accessible by tuning the top-gate voltage, V_G , in the range -3 V to -4 V for both devices. Over this same range, normal-state sheet resistance R_N , measured above the critical temperature $T_{c0} \sim 1.6$ K of the Al islands, spanned $R_N \sim 100 \Omega$ at $V_G \sim -3$ V to $R_N \sim 1 \text{ M}\Omega$ at $V_G \sim -4$ V, as shown in Fig. 1.

The experimental phase diagram in the T - V_G plane is shown in Fig. 1, along with representative $R_s(T)$ curves at fixed V_G . In the superconducting (S) region, with $R_N \lesssim 1 \text{ k}\Omega$, all $R_s(T)$ curves were found to decrease with lower T down to the smallest measurable resistance, $R_s \sim 0.1 \Omega$. At more negative gate voltages, in the region marked M^* , R_s initially falls, then saturates at a V_G -dependent value ranging from $\sim 1 \Omega$ up to $\sim R_Q$. As discussed below, $R_s(T)$ curves in M^* are distinct from those in S throughout the temperature range. In particular, $R_s(T)$ in M^* is not well described by the BKT form [20]. Comparable to the conventional SIT, the M^* -I separatrix (orange curve in Fig. 1) occurs at $R_s \sim R_Q$ and is roughly independent of T from lowest measured temperature up to T_{c0} . At more negative V_G beyond the M^* -I separatrix in the region marked I, $R_s(T)$ rises with lower T , characteristic of the insulating phase. We have previously investigated variable range hopping and activated regimes of the I phase, and did not observe low- T saturation I phase away from M^* -I separatrix [16]. Note in Fig. 1 that R_N slightly exceeds $R_s(T)$ just below T_{c0} throughout the measured S, M^* , and I phases, so that the transition at T_{c0} makes a small upward step in resistance going from below to above the transitions where the islands become normal. The critical temperature for the islands, $T_{c0} \sim 1.6$ K, is independent of V_G .

Representative $R_s(T)$ curves are shown in Fig. 1. For a larger set of curves, finely sampled in V_G throughout the S and M^* phases, we fit $R_s(T)$ to the BKT form [20, 21],

$$R_s(T) = aR_N \exp \left[-b \left(\frac{T_{c0} - T}{T - T_{\text{BKT}}} \right)^{1/2} \right]. \quad (1)$$

For each V_G , a least-square fit to the logarithm of $R_s(T)$ yields a , b , and T_{BKT} as fit parameters, with $T_{c0} = 1.6$ K and $R_N(V_G)$ taken from measurements. Figure 2(a) shows a typical fit deep in the S regime, yielding excellent agreement between experimental and Eq. 1 over several orders of magnitude of $R_s(T)$ from the lowest measured resistance to R_N . The resulting T_{BKT} is indicated along the top axis. As V_G is set more negative

but still within S, the data and fits begin to deviate most noticeably for $T \lesssim 1$ K. Note that the measurement lies *below* the fit, in contrast to [24]. The extracted T_{BKT} values, marked on the top axes of Figs. 2(b,c), move quickly toward zero as the S-M* boundary is approached at more negative gate voltages.

Repeating fits across a range of gate voltages within the S region yields the values for T_{BKT} shown in Fig. 2(d), plotted as a function of R_N^{-1} , along with a classical model (absent charging effects), $T_{\text{BKT}} \propto R_N^{-1}$. We find that T_{BKT} is roughly proportional to R_N^{-1} in the S region, but deviates below the model line, reaching $T_{\text{BKT}} = 0$ at a value of $R_N(V_G) \sim 1$ k Ω , coinciding with the S-M* boundary. We emphasize that value of V_G marked as the the S-M* boundary in Fig. 2 was defined by the separatrix (blue trace) in Fig. 1, not by the point where $T_{\text{BKT}} = 0$. The observation that T_{BKT} reaches zero at the S-M* boundary is a striking experimental result, not expected within a conventional SIT picture, where $T_{\text{BKT}} \rightarrow 0$ at $R_s \sim R_Q$, i.e., the M*-I boundary in this case.

The simple proportionality $T_{\text{BKT}} = \gamma R_N^{-1}$ follows from the Ambegaokar-Baratoff relation at $T \ll \Delta$ for individual junctions, $I_c^{(i)} R_N^{(i)} = \pi \Delta / 2e$, where Δ is the superconducting gap induced in the InAs under the Al islands. Setting $R_N = R_N^{(i)}$ and $E_J = (\hbar/2e) I_c^{(i)}$ gives $E_J = (\Delta/2)(R_Q/R_N)$. The classical BKT relation, $k_B T_{\text{BKT}} = (\pi/2) E_J$ [33] can then be written $T_{\text{BKT}} = (\pi \Delta / 4k_B)(R_Q/R_N)$.

An upper bound on Δ based on the critical temperature of the Al islands gives $\Delta \lesssim 1.76 k_B T_{c0} = 240 \mu\text{eV}$, using the measured $T_{c0} = 1.6$ K. A lower bound based on the $I_c R_N$ product, using the array depinning current $I_d^{(A)} = 20 \mu\text{A} \lesssim 40 I_c^{(i)}$ of the 40-junction-wide array at $R_N = 0.4$ k Ω , gives $\Delta \gtrsim 120 \mu\text{eV}$ [16]. Tunneling spectroscopy into the InAs adjacent to the Al edge in similar material yields $\Delta \sim 190 \mu\text{eV}$ [34]. Using this value gives $\gamma = (\pi \Delta / 4k_B) R_Q \sim 11$ k Ω K.

Experimentally, we observe the proportionality $T_{\text{BKT}} = \gamma^{(\text{exp})} R_N^{-1}$ in the S phase, as seen in Fig. 2(d), but with a considerably smaller slope, $\gamma^{(\text{exp})} \sim 0.2$ k Ω K. We interpret the discrepancy as reflecting a suppressed BKT transition temperature, $T_{\text{BKT}} \sim 0.02 E_J$ —while keeping $E_J \sim (\Delta/2)(R_Q/R_N)$ —instead of the classical relation $T_{\text{BKT}} \sim E_J$. This interpretation is consistent with a charging energy $E_C \sim 150 \mu\text{eV}$, previously measured in the I phase [16], being comparable to E_J when $R_s \sim R_N \sim R_Q$.

As V_G becomes more negative, moving the system from the S phase toward the S-M* boundary, T_{BKT} deviates from the proportionality $T_{\text{BKT}} = \gamma R_N^{-1}$, reaching zero (roughly linearly) at the S-M* boundary, as seen in Fig. 2(d). In conventional SIT systems, reduction of T_{BKT} below $\sim E_J \propto R_N^{-1}$ is an expected and well investigated consequence of quantum corrections associated

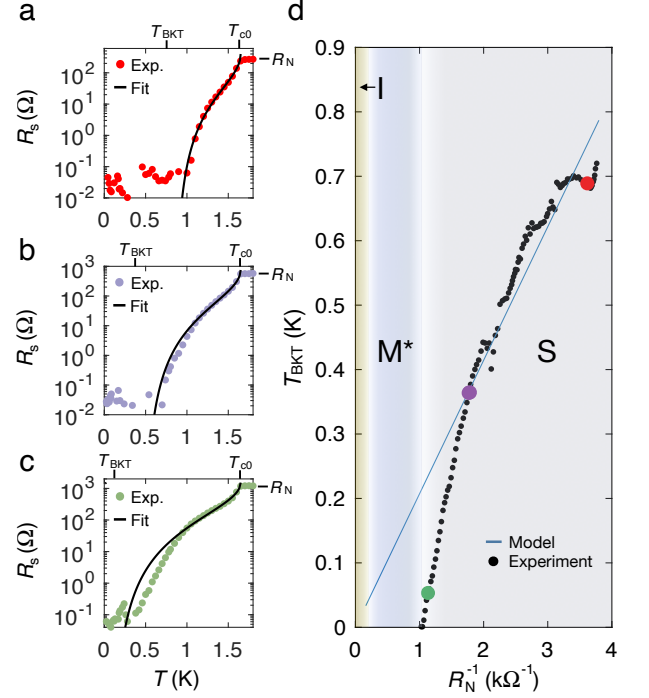


FIG. 2. (a-c) Sheet resistance, $R_s(T)$ as a function of temperature, T at three gate voltages (filled colored circles), parameterized by normal-state sheet resistance, R_N , along with fits to Eq. 1. Top axes show gate-independent critical temperature, T_{c0} of the Al squares, read directly from the data, and BKT transition temperature, T_{BKT} from the fits. Note the good fit deep in S, which becomes poorer toward the S-M* boundary. (d) BKT transition temperature T_{BKT} extracted from fits at many gate voltages (black filled circles), as a function of R_N^{-1} . T_{BKT} reaches zero near the S-M* boundary, defined by the blue separatrix in Fig. 1. Three colored data points correspond to panels a-c. Model line is based on linear relations $T_{\text{BKT}} \sim E_J \propto I_c \propto R_N^{-1}$, with a single fit parameter (see text).

with island capacitance [1, 2, 35, 36]. However, in the conventional case, the suppressed T_{BKT} reaches zero at the SIT, where $R_N \sim R_Q$. In the present case, one might have expected a deviation of T_{BKT} to reach zero at the corresponding M*-I separatrix where $R_s \sim R_N \sim R_Q$, but that is not what is observed. Instead, we find that T_{BKT} reaches zero at the S-M* boundary, and that $T_{\text{BKT}} = 0$ throughout the M* phase.

These observation, the 50-fold reduction in slope of T_{BKT} versus R_N^{-1} in the S phase and the vanishing of T_{BKT} in the M* phase, suggest a picture of vortex-antivortex binding that is suppressed in S and fails in M*. As discussed below, this picture is consistent with the observed scaling in M* of R_s with small perpendicular magnetic field.

The observed vanishing of T_{BKT} at the S-M* boundary is consistent with another method of determining T_{BKT} : a jump in the voltage-current characteristic, $V \propto I^\zeta$,

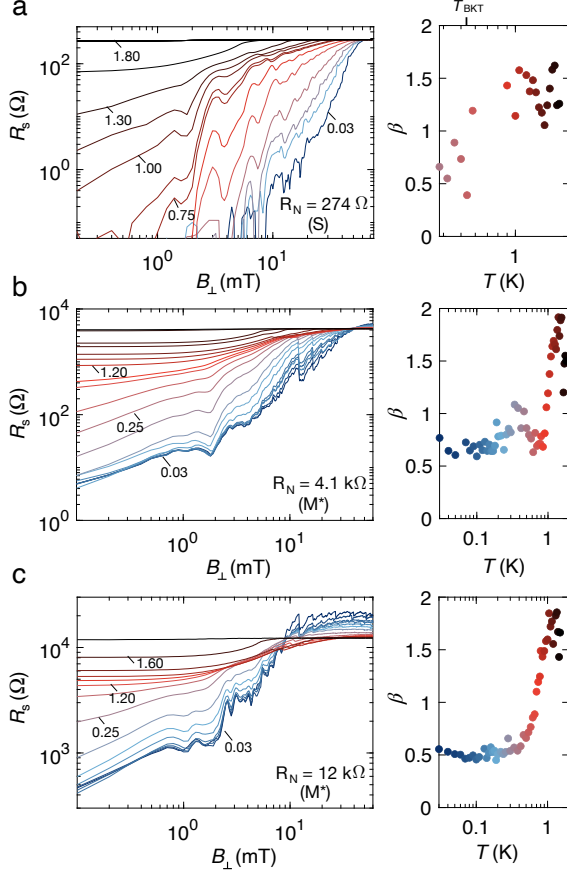


FIG. 3. Low-field magnetoresistance $R_s(B_\perp, T)$ as a function of perpendicular magnetic field, B_\perp , shows a power-law dependence (straight line on a log-log plot), $R_s(B_\perp, T) - R_s(0, T) = A(T)B_\perp^{\beta(T)}$ with a power $\beta(T)$ dependence on temperature, T (marked on graphs), and gate-controlled normal-state sheet resistance, R_N . (a) In the superconducting (S) phase, on the low-resistance (less negative V_G) side of the S-M* boundary, with $R_N = 274 \Omega$, $\beta(T_{\text{BKT}}) \sim 1$. (b-c) In M*, $\beta(T) < 1$ at low T , and appears to settle around $\beta \sim 1/2$. Fluctuations in $R_s(B_\perp)$ on a ~ 1 mT scale result from flux commensuration effects.

from ohmic, $\zeta = 1$, for $T > T_{\text{BKT}}$ to $\zeta = 3$ at $T = T_{\text{BKT}}$. The condition $\zeta = 3$ is equivalent to the point where $R_s \propto dV/dI \propto V^{\zeta-1}$ first touches zero at its minimum at zero bias. Because R_s is an even function of I , when it first touches zero it will in general be parabolic to lowest order, $R_s \propto I^2$, which is equivalent to $V \propto I^3$. Throughout M*, the nonzero R_s down to the lowest temperatures implies ohmic response, $\zeta = 1$. The condition $\zeta = 3$ is never reached in M*, consistent with $T_{\text{BKT}} = 0$.

By the same argument, now in the S phase, T_{BKT} is roughly where $R_s \propto V^{\zeta-1}$ first touches zero. That is, R_s will be parabolic ($\zeta - 1 \sim 2$) at T_{BKT} . Below T_{BKT} , dV/dI will be a flat-bottomed, even function around zero bias, giving $\zeta \geq 5$. Above T_{BKT} , the ohmic R_s gives $\zeta = 1$. This implies a jump from $\zeta = 1$ to $\zeta \sim 3$ at T_{BKT} in the S phase.

We next examine magnetoresistance $R_s(B_\perp)$ at small perpendicular magnetic field, B_\perp , which has been investigated previously to identify the BKT transition in arrays and 2D films. Conventional SITs [29, 37, 38] and anomalous metals [22, 23, 32, 39] often show a power-law dependence, $R_s(B_\perp, T) - R_s(0, T) = A(T)B_\perp^{\beta(T)}$, in some cases consistent the BKT prediction, $\beta(T_{\text{BKT}}) = 1$ [29, 32, 37]. Other experiments [38] find $\beta(T) > 1$, consistent with activated vortex creep with logarithmic vortex interactions [40]. In systems exhibiting anomalous metal behavior [$R_s(0, 0) \neq 0$], magnetic field dependence of the low- T saturating resistance was observed to be activated [41] or power-law with $1 < \beta(T) < 3$ in MoGe films [42] and crystalline NbS₂ [39]. In higher-resistance granular InO₂ films, smaller exponents were found, $\beta(T \rightarrow 0) = 0.66$ [22] and $\beta(T \rightarrow 0) = 0.45$ [23] in granular films. Reference [43] reports $\beta(T) \sim 2$, also consistent with [42], though their lowest temperature data appears to show $\beta(T) < 1$.

Figure 3 shows $R_s(B_\perp, T)$ at several temperatures, in the S and M* phases, along with best-fit values for $\beta(T)$ for each T to the form $R_s(B_\perp, T) - R_s(0, T) = A(T)B_\perp^{\beta(T)}$, with prefactor $A(T)$. The power-law can be seen at the lowest fields, less than one flux quantum per plaquette $[(h/2e)(a+b)^{-2} \sim 2 \text{ mT}]$, modulated by flux-commensuration effects above $\sim 2 \text{ mT}$. In the S phase [Fig. 3(a)], $\beta(T) \sim 1$ for $T \sim T_{\text{BKT}} \sim 0.5 \text{ K}$, roughly consistent with results in Fig. 2(d) for similar R_N . We note without explanation that the trend of increasing $\beta(T)$ with temperature is opposite of the trend reported in [29]. In the S phase, $R_s(B_\perp)$ for $T < T_{\text{BKT}}$ is below the experimental noise floor.

Throughout the M* phase, where $T_{\text{BKT}} = 0$, we find $\beta(T) < 1$ at low-temperatures (noting a bump to $\beta \sim 1$ around 0.5 K in Fig. 3(b), close the S-M* boundary). Near the M*-I border, $\beta \sim 1/2$ for a broad range of temperatures similar to [23, 43].

We speculate that the observed β reflects incomplete binding of vortex-antivortex pairs in M*. Within this picture, the value of coupling constant $K = J/k_B T$ where vortex-antivortex pairs form, but fail to bind, is $1/\pi$ [18, 44]. Then, the relation $\beta = \pi K/2$ [29] gives $\beta = 1/2$. In the S phase, on the other hand, vortex-antivortex pairs bind at T_{BKT} , giving $\beta = 1$.

Applying an in-plane magnetic field, B_\parallel suppresses the M* phase, restoring a conventional SIT, though with a small and field-dependent scaling exponent, as shown in Fig. 4. In Ref. [16], we speculated that the suppression of the M* phase with in-plane field results from increased dissipation from the soft superconducting gap, which stabilizes phase fluctuations, in this case caused by the softening of the induced gap by the in-plane field [34, 45]. This interpretation differs from Ref. [12], which found that galvanic (though not capacitive [46]) coupling to a

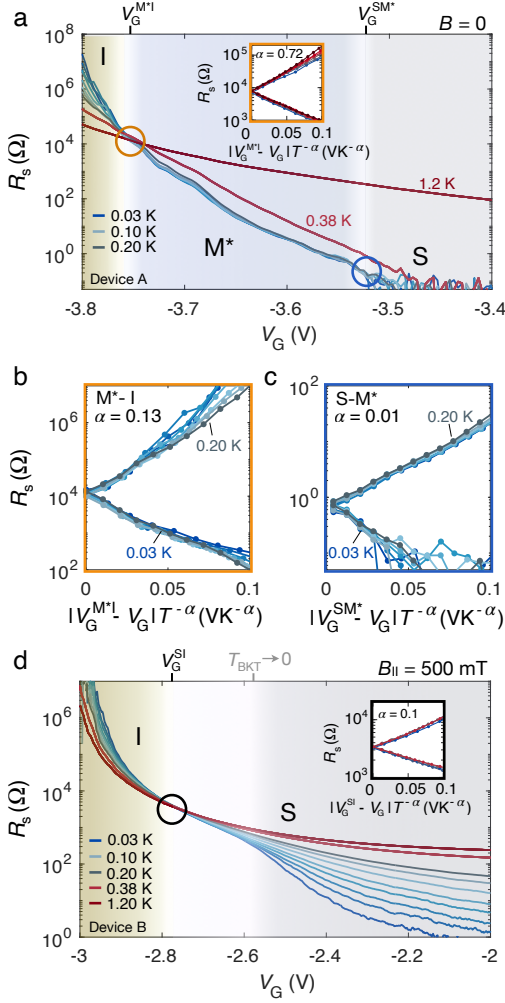


FIG. 4. (a) Sheet resistance, R_s , as a function of gate voltage, V_G at $B_{\parallel} = B_{\perp} = 0$ shows T -independent curves at low T across the anomalous metal phase, M^* , which flair out for different T in the superconducting (S) and insulating (I) phases. Inset: Scaling using only high- T isotherms ($T > 0.2$ K) at the M^* -I boundary (orange circle in main panel) yields exponent $\alpha = 0.72$. (b) Scaling using only low- T isotherms ($T < 0.2$ K) at the M^* -I boundary yields $\alpha = 0.13$. (c) Scaling at the S- M^* boundary [blue circle in (a)], yields $\alpha = 0.01$. (d) Applying an in-plane magnetic field, $B_{\parallel} = 0.5$ T, results in a single crossing of isotherms (black circle). Inset: Scaling with all isotherms yields $\alpha = 0.1$. We interpret the small α , i.e., nearly parallel isotherms, as a vestige of M^* , where low- T isotherms coincide. The broad S-I transition (white region) is bounded by the crossing point on the I side and the rapid spreading of isotherms on the S side. The top axis indicates where $T_{\text{BKT}} \rightarrow 0$ following similar analysis to Fig. 2. Data for Device B.

dissipative channel induces rather than suppressed the anomalous metal phase. Stabilization of superconductivity with in-plane field has been reported in a variety of 2D systems, including $\text{LaAlO}_3/\text{SrTiO}_3$ interfaces [47] as well as Pb [47, 48] and WTe_2 [49] thin films. Stabilization of superconductivity by an in-plane field has been

attributed to mechanisms besides dissipation, including the compensation [50] and freezing [51] of magnetic impurities. Similar stabilization of superconductivity by an applied magnetic field was also found in 1D nanowires, where it was also attributed to dissipation induced by the applied field [52, 53]. Scaling analysis for conventional SITs can be applied to a gate-voltage controlled transition using the scaled voltage axis, $|V_G^{S-I} - V_G|T^{-\alpha}$, with scaling exponent $\alpha = (z\nu)^{-1}$ where ν and z are spatial and dynamical exponents [2, 16]. Using B_{\parallel} to eliminate the M^* phase, we examine $\alpha(B_{\parallel})$ of the S- M^* , M^* -I (Fig. 4(a-c)) and S-I (Fig. 4(d)) transitions. For the M^* -I transition (orange circle) using only higher temperature data ($T > 0.2$ K) yields $\alpha = 0.72$ consistent with classical percolation, $z\nu = 4/3$ [16] while low- T scaling (Fig. 4(b)), yields $\alpha = 0.13$. Scaling at the S- M^* boundary, (blue circle), defined by the S- M^* separatrix in Fig. 1, coinciding with the value of V_G where $T_{\text{BKT}} \rightarrow 0$, also yields a small value, $\alpha(B_{\parallel} = 0) = 0.01$ (Fig. 4(c)). The reduced value of α is not surprising since within the M^* phase, $dR_s/dT \rightarrow 0$ which yields $\alpha \rightarrow 0$ on the M^* side of the transition.

Applying an in-plane field causes the S- M^* and M^* -I boundaries to coalesce, eliminating a clear M^* phase (Fig. 4(d)). Scaling at the remaining single crossing of isotherms yields a small exponent $\alpha(B_{\parallel} = 0.5\text{ T}) \sim 0.10$. At the extended S-I crossing at nonzero B_{\parallel} isotherms diverge only weakly. The single crossing in Fig. 4(d) is the remnant of the M^* -I crossing at $B_{\parallel} = 0$ [orange circle in Fig. 4(a)], where low- T isotherms diverge on the I side but remain parallel in M^* , only to diverge again at the remote S- M^* boundary (blue circle). We do not interpret the small α as a Griffiths transition [54–56], though cannot rule it out. Rather, we interpret the small α as a vestige of the M^* phase, where α vanishes on the M^* sides of the S- M^* and M^* -I boundaries.

We thank A. Kapitulnik, S. Kivelson, and B. Spivak for useful discussion. Research supported by the Danish National Research Foundation, Microsoft, and a research grant (Project 43951) from VILLUM FONDEN.

* Present Address: Department of Applied Physics, Yale University, New Haven, CT, 06520, USA.
Email: charlotte.boettcher@yale.edu

† Present Address: IBM Research Laboratory, Zürich, Zürich, Switzerland

‡ Present Address: New York University, New York, NY 10003, USA

[1] R. S. Newrock, C. J. Lobb, U. Geigenmüller, and M. Octavio, *The Two-Dimensional Physics of Josephson Junction Arrays*, Solid State Physics, Vol. 54 (1999) pp. 263–512.

- [2] Rosario Fazio and Herre van der Zant, “Quantum phase transitions and vortex dynamics in superconducting networks,” *Physics Reports* **355**, 235–334 (2001).
- [3] Vsevolod F. Gantmakher and Valery T. Dolgoplov, “Superconductor-insulator quantum phase transition,” *Physics-Uspekhi* **53**, 1–49 (2010).
- [4] Yen-Hsiang Lin, J. Nelson, and A.M. Goldman, “Superconductivity of very thin films: The superconductor–insulator transition,” *Physica C: Superconductivity and its Applications* **514**, 130–141 (2015).
- [5] Andrew D. King, Juan Carrasquilla, Jack Raymond, Isil Ozfidan, Evgeny Andriyash, Andrew Berkley, Mauricio Reis, Trevor Lanting, Richard Harris, Fabio Altomare, Kelly Boothby, Paul I. Bunyk, Colin Enderud, Alexandre Fréchet, Emile Hoskinson, Nicolas Ladizinsky, Travis Oh, Gabriel Poulin-Lamarre, Christopher Rich, Yuki Sato, Anatoly Yu. Smirnov, Loren J. Swenson, Mark H. Volkmann, Jed Whittaker, Jason Yao, Eric Ladizinsky, Mark W. Johnson, Jeremy Hilton, and Mohammad H. Amin, “Observation of topological phenomena in a programmable lattice of 1,800 qubits,” *Nature* **560**, 456–460 (2018).
- [6] Daniel Leykam, Alexei Andreanov, and Sergej Flach, “Artificial flat band systems: from lattice models to experiments,” *Advances in Physics: X* **3**, 1473052 (2018).
- [7] L. B. Ioffe, M. V. Feigel’man, A. Ioselevich, D. Ivanov, M. Troyer, and G. Blatter, “Topologically protected quantum bits using Josephson junction arrays,” *Nature* **415**, 503–506 (2002).
- [8] B. Douçot and L. B. Ioffe, “Physical implementation of protected qubits,” *Reports on Progress in Physics* **75**, 072001 (2012).
- [9] Sudip Chakravarty, Steven Kivelson, Gergely T. Zimanyi, and Bertrand I. Halperin, “Effect of quasiparticle tunneling on quantum-phase fluctuations and the onset of superconductivity in granular films,” *Physical Review B* **35**, 7256–7259 (1987).
- [10] Matthew P. A. Fisher, “Quantum phase transitions in disordered two-dimensional superconductors,” *Physical Review Letters* **65**, 923–926 (1990).
- [11] Aharon Kapitulnik, Steven A. Kivelson, and Boris Spivak, “Colloquium: Anomalous metals: Failed superconductors,” *Reviews of Modern Physics* **91**, 011002 (2019).
- [12] Aharon Kapitulnik, Nadya Mason, Steven A. Kivelson, and Sudip Chakravarty, “Effects of dissipation on quantum phase transitions,” *Physical Review B* **63**, 125322 (2001).
- [13] Philip Phillips and Denis Dalidovich, “The Elusive Bose Metal,” *Science* **302**, 243–247 (2003).
- [14] M. C. Diamantini, A. Yu. Mironov, S. M. Postolova, X. Liu, Z. Hao, D. M. Silevitch, Ya. Kopelevich, P. Kim, C. A. Trugenberger, and V. M. Vinokur, “Bosonic topological insulator intermediate state in the superconductor-insulator transition,” *Physics Letters A* **384**, 126570 (2020).
- [15] Benjamin Sécépé, Mikhail Feigel’man, and Teunis M. Klapwijk, “Quantum breakdown of superconductivity in low-dimensional materials,” *Nature Physics* **16**, 734–746 (2020).
- [16] C. G. L. Böttcher, F. Nichele, M. Kjaergaard, H. J. Suominen, J. Shabani, C. J. Palmstrøm, and C. M. Marcus, “Superconducting, insulating and anomalous metallic regimes in a gated two-dimensional semiconductor-superconductor array,” *Nature Physics* **14**, 1138–1144 (2018).
- [17] Jorge V. José, *40 Years of Berezinskii-Kosterlitz-Thouless Theory* (World Scientific, 2013).
- [18] J Michael Kosterlitz, “Kosterlitz–Thouless physics: a review of key issues,” *Reports on Progress in Physics* **79**, 026001 (2016).
- [19] Victor Drouin-Touchette, “The Kosterlitz–Thouless phase transition: an introduction for the intrepid student,” arXiv/2207.13748 (2022).
- [20] B. I. Halperin and David R. Nelson, “Resistive transition in superconducting films,” *Journal of Low Temperature Physics* **36**, 599–616 (1979).
- [21] A. M. Kadin, K. Epstein, and A. M. Goldman, “Renormalization and the Kosterlitz–Thouless transition in a two-dimensional superconductor,” *Physical Review B* **27**, 6691–6702 (1983).
- [22] Xinyang Zhang, Bar Hen, Alexander Palevski, and Aharon Kapitulnik, “Robust anomalous metallic states and vestiges of self-duality in two-dimensional granular In-InOx composites,” *npj Quantum Materials* **6**, 30 (2021).
- [23] Xinyang Zhang, Alexander Palevski, and Aharon Kapitulnik, “Anomalous metals: From failed superconductor to failed insulator,” *Proceedings of the National Academy of Sciences* **119**, e2202496119 (2022).
- [24] Yen-Hsiang Lin, J. Nelson, and A. M. Goldman, “Suppression of the Berezinskii–Kosterlitz–Thouless Transition in 2D Superconductors by Macroscopic Quantum Tunneling,” *Physical Review Letters* **109**, 017002 (2012).
- [25] Sungyu Park, Junghyun Shin, and Eunseong Kim, “Scaling analysis of field-tuned superconductor–insulator transition in two-dimensional tantalum thin films,” *Scientific Reports* **7**, 42969 (2017).
- [26] I. Tamir, A. Benyamini, E. J. Telford, F. Gorniaczyk, A. Doron, T. Levinson, D. Wang, F. Gay, B. Sécépé, J. Hone, K. Watanabe, T. Taniguchi, C. R. Dean, A. N. Pasupathy, and D. Shahar, “Sensitivity of the superconducting state in thin films,” *Science Advances* **5**, eaau3826 (2019).
- [27] Matthew P. A. Fisher, “Quantum Phase Slips and Superconductivity in Granular Films,” *Physical Review Letters* **57**, 885–888 (1986).
- [28] C. D. Chen, P. Delsing, D. B. Haviland, Y. Harada, and T. Claeson, “Scaling behavior of the magnetic-field-tuned superconductor-insulator transition in two-dimensional Josephson-junction arrays,” *Physical Review B* **51**, 15645–15648 (1995).
- [29] C. D. Chen, P. Delsing, D. B. Haviland, Y. Harada, and T. Claeson, “Flux flow and vortex tunneling in two-dimensional arrays of small Josephson junctions,” *Physical Review B* **54**, 9449–9457 (1996).
- [30] Nadya Mason and Aharon Kapitulnik, “True superconductivity in a two-dimensional superconducting-insulating system,” *Physical Review B* **64**, 060504 (2001).
- [31] Yu Saito, Yuichi Kasahara, Jianting Ye, Yoshihiro Iwasa, and Tsutomu Nojima, “Metallic ground state in an ion-gated two-dimensional superconductor,” *Science* **350**, 409–413 (2015).
- [32] Zhuoyu Chen, Bai Yang Wang, Adrian G. Swartz, Hyeok Yoon, Yasuyuki Hikita, Srinivas Raghu, and Harold Y. Hwang, “Universal behavior of the bosonic metallic ground state in a two-dimensional superconductor,” *npj Quantum Materials* **6**, 15 (2021).
- [33] M Tinkham, *Introduction to Superconductivity* (2004).

- [34] M. Kjaergaard, F. Nichele, H. J. Suominen, M. P. Nowak, M. Wimmer, A. R. Akhmerov, J. A. Folk, K. Flensberg, J. Shabani, C. J. Palmström, and C. M. Marcus, “Quantized conductance doubling and hard gap in a two-dimensional semiconductor-superconductor heterostructure,” *Nature Communications* **7**, 12841 (2016).
- [35] Jorge V. Jose and Cristian Rojas, “Superconducting to normal state phase boundary in arrays of ultrasmall Josephson junctions,” *Physica B-Condensed Matter*, 1–9 (1994).
- [36] H. S. J. van der Zant, W. J. Elion, L. J. Geerligs, and J. E. Mooij, “Quantum phase transitions in two dimensions: Experiments in Josephson-junction arrays,” *Physical Review B* **54**, 10081–10093 (1996).
- [37] S. Martin, A. T. Fiory, R. M. Fleming, G. P. Espinosa, and A. S. Cooper, “Vortex-Pair Excitation near the Superconducting Transition of Bi₂Sr₂CaCu₂O₈ Crystals,” *Physical Review Letters* **62**, 677–680 (1989).
- [38] G. Sambandamurthy, A. Johansson, E. Peled, D. Shahar, P. G. Björnsson, and K. A. Moler, “Power law resistivity behavior in 2D superconductors across the magnetic field-tuned superconductor-insulator transition,” *Europhysics Letters* **75**, 611–617 (2007).
- [39] A. W. Tsen, B. Hunt, Y. D. Kim, Z. J. Yuan, S. Jia, R. J. Cava, J. Hone, P. Kim, C. R. Dean, and A. N. Pasupathy, “Nature of the quantum metal in a two-dimensional crystalline superconductor,” *Nature Physics* **12**, 208–212 (2016).
- [40] M. V. Feigel’man, V. B. Geshkenbein, and A. I. Larkin, “Pinning and creep in layered superconductors,” *Physica C: Superconductivity* **167**, 177–187 (1990).
- [41] D. Ephron, A. Yazdani, A. Kapitulnik, and M. R. Beasley, “Observation of Quantum Dissipation in the Vortex State of a Highly Disordered Superconducting Thin Film,” *Physical Review Letters* **76**, 1529–1532 (1995).
- [42] Jiansheng Wu and Philip Phillips, “Vortex glass is a metal: Unified theory of the magnetic-field and disorder-tuned Bose metals,” *Physical Review B* **73**, 214507 (2006).
- [43] Linjun Li, Chuan Chen, Kenji Watanabe, Takashi Taniguchi, Yi Zheng, Zhuan Xu, Vitor M. Pereira, Kian Ping Loh, and Antonio H. Castro Neto, “Anomalous Quantum Metal in a 2D Crystalline Superconductor with Electronic Phase Nonuniformity,” *Nano Letters* **19**, 4126–4133 (2019).
- [44] Sara A. Solla and Eberhard K. Riedel, “Vortex excitations and specific heat of the planar model in two dimensions,” *Phys. Rev. B* **23**, 6008–6012 (1981).
- [45] Abhishek Banerjee, Abhinab Mohapatra, R. Ganesan, and P. S. Anil Kumar, “Restoring Superconductivity in the Quantum Metal Phase of NbSe₂ Using Dissipative Coupling,” *Nano Letters* **19**, 1625–1631 (2019).
- [46] Nadya Mason and Aharon Kapitulnik, “Superconductor-insulator transition in a capacitively coupled dissipative environment,” *Physical Review B* **65**, 220505 (2002).
- [47] H. Jeffrey Gardner, Ashwani Kumar, Liuqi Yu, Peng Xiong, Maitri P. Warusawithana, Luyang Wang, Oskar Vafek, and Darrell G. Schlom, “Enhancement of superconductivity by a parallel magnetic field in two-dimensional superconductors,” *Nature Physics* **7**, 895–900 (2011).
- [48] Masato Niwata, Ryuichi Masutomi, and Tohru Okamoto, “Magnetic-Field-Induced Superconductivity in Ultrathin Pb Films with Magnetic Impurities,” *Physical Review Letters* **119**, 257001 (2017).
- [49] Tomoya Asaba, Yongjie Wang, Gang Li, Ziji Xiang, Colin Tinsman, Lu Chen, Shangnan Zhou, Songrui Zhao, David Laleyan, Yi Li, Zetian Mi, and Lu Li, “Magnetic Field Enhanced Superconductivity in Epitaxial Thin Film WTe₂,” *Scientific Reports* **8**, 6520 (2018).
- [50] V. Jaccarino and M. Peter, “Ultra-High-Field Superconductivity,” *Physical Review Letters* **9**, 290–292 (1962).
- [51] M. Yu. Kharitonov and M. V. Feigelman, “Enhancement of superconductivity in disordered films by parallel magnetic field,” *Journal of Experimental and Theoretical Physics Letters* **82**, 421–425 (2005).
- [52] Mingliang Tian, Nitesh Kumar, Shengyong Xu, Jinguo Wang, James S. Kurtz, and M. H. W. Chan, “Suppression of Superconductivity in Zinc Nanowires by Bulk Superconductors,” *Physical Review Letters* **95**, 076802 (2005).
- [53] Henry C. Fu, Alexander Seidel, John Clarke, and Dung-Hai Lee, “Stabilizing Superconductivity in Nanowires by Coupling to Dissipative Environments,” *Physical Review Letters* **96**, 157005 (2006).
- [54] Ying Xing, Hui-Min Zhang, Hai-Long Fu, Haiwen Liu, Yi Sun, Jun-Ping Peng, Fa Wang, Xi Lin, Xu-Cun Ma, Qi-Kun Xue, Jian Wang, and X. C. Xie, “Quantum Griffiths singularity of superconductor-metal transition in Ga thin films,” *Science* **350**, 542–545 (2015).
- [55] Yi Liu, Ziqiao Wang, Pujia Shan, Yue Tang, Chaoferi Liu, Cheng Chen, Ying Xing, Qingyan Wang, Haiwen Liu, Xi Lin, X. C. Xie, and Jian Wang, “Anomalous quantum Griffiths singularity in ultrathin crystalline lead films,” *Nature Communications* **10**, 3633 (2019).
- [56] Xiaowen Han, Yufeng Wu, Hong Xiao, Miao Zhang, Min Gao, Yi Liu, Jian Wang, Tao Hu, Xiaoming Xie, and Zengfeng Di, “Disorder-Induced Quantum Griffiths Singularity Revealed in an Artificial 2D Superconducting System,” *Advanced Science* **7**, 1902849 (2020).